JACS
JOURNAL OF THE AMERICAN CHEMICAL SOCIETY

Communication

pubs.acs.org/JACS

Nickel–Silicide Colloid Prepared under Mild Conditions as a Versatile Ni Precursor for More Efficient CO_2 Reforming of CH_4 Catalysts

David Baudouin,[‡,§,†] Kaï Chung Szeto,[‡] Pierre Laurent,[‡] Aimery De Mallmann,[‡] Bernard Fenet,[⊥,∥] Laurent Veyre,[‡] Uwe Rodemerck,[5] Christophe Copéret,*[,‡,§,†] and Chloé Thieuleux*[,‡]

[‡]Université de Lyon, ICL, C2P2 UMR 5265, CPE Lyon, 43 Bd du 11 Novembre 1918, F-69616 Villeurbanne, France

[§]Department of Chemistry, ETH Zürich, HCI H 206, Wolfgang-Pauli-Strasse 10, CH-8093 Zürich, Switzerland

[⊥]Centre Commun de RMN, Université de Lyon, 69003 Lyon, France

[∥]Université Lyon 1 Claude Bernard, ESCPE Lyon, 43, Bd du 11 Novembre 1918, 69616 Villeurbanne Cedex, France

[5]Leibniz Institute for Catalysis at University Rostock, Albert-Einstein-Straße 29a, D-18059 Rostock, Germany

Supporting Information

ABSTRACT: Preparing highly active and stable non-noble-metal-based dry reforming catalysts remains a challenge today. In this context, supported nickel nanoparticles with sizes of 1.3 ± 0.2 and 2.1 ± 0.2 nm were synthesized on silica and ceria, respectively, via a two-step colloidal approach. First, 2-nm nickel–silicide colloids were synthesized from $Ni(COD)_2$ and octylsilane at low temperature; they were subsequently dispersed onto supports prior to reduction under H_2. The resulting catalysts display high activity in dry reforming compared to their analogues prepared using conventional approaches, ceria providing greatly improved catalyst stability.

Steam reforming of natural gas is the major process used to generate syngas in industry because of its high H_2/CO ratio (R = 3, eq 1). This ratio needs to be tuned for off-stream processes, such as Fischer–Tropsch,[1−3] and CO_2 reforming (dry reforming, DR) can thus be used to provide a lower H_2/CO ratio (R = 1; eq 2).[4]

$$CH_4 + H_2O \leftrightarrows CO + 3H_2 \quad (1)$$

$$CH_4 + H_2O \leftrightarrows 2CO + 2H_2 \quad (2)$$

Catalysts for this reaction are based on supported nanoparticles, and nickel-based catalytic systems are preferred to noble metals for economic reasons, despite their lower stability.[5−9] However, after tremendous research efforts,[10−13] increasing nickel dispersion above 35–50% (i.e., a diameter of 2–3 nm) and improving their stability remain challenging.

The development of a general approach for catalyst preparation, which would be applicable to several supports, remains therefore of great interest in view of improving the efficiency and cost-effectiveness of a catalytic process.[14]

Here, we describe a versatile method to prepare small Ni nanoparticles on oxide supports via a colloidal approach. It involves the preparation of nickel–silicide colloids [Ni_xSi–C_8H_{17}] with a narrow size distribution (2.4 ± 0.5 nm after oxidation) by reaction of Ni(1,5-cyclooctadiene)$_2$ with octylsilane in the presence of H_2 (Figure 1), which are then dispersed on an oxide support to generate small supported Ni nanoparticles (1.3 ± 0.2 nm on silica and 2.1 ± 0.2 nm on ceria). Both systems display high activity under low-temperature DR conditions, ceria providing much greater stability.

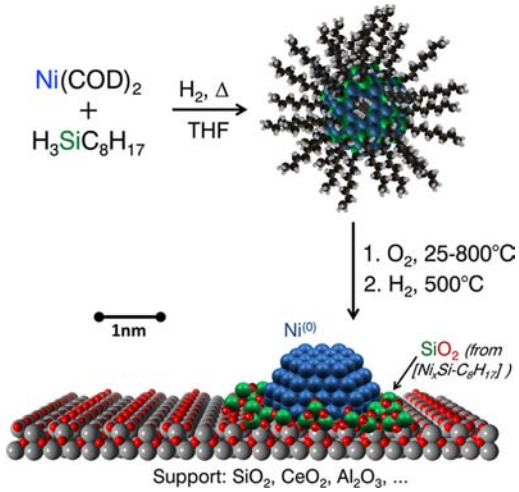

Figure 1. Synthesis of nickel–silicide colloids and their conversion into supported Ni catalysts.

The nickel–silicide colloids were obtained by contacting a solution of $Ni(COD)_2$ in THF with octylsilane under H_2 (3 bar) at 55–65 °C.[15,16] This protocol yields a deep black colloidal solution, [Ni_xSi–C_8H_{17}], presenting an outstanding stability toward sedimentation (no evolution after 2 months under Ar). The formation of these colloids was first investigated by solution NMR spectroscopy (Figure S1). The signals associated with the starting Ni precursor, Ni(C_8H_{12})$_2$ (2.15 and 4.35 ppm), as well as the one corresponding to H_3Si-R (3.51 ppm), decreased significantly with reaction time, disappearing after 15 and 3.5 h, respectively. The full consumption of H_3Si– during the reaction was confirmed by infrared spectroscopy of the colloidal solution (Figure S2).

The quantitative consumption of $Ni(COD)_2$ and the silane hydrides occurred in parallel to the production of cyclooctane

Received: November 14, 2012
Published: December 10, 2012

   dx.doi.org/10.1021/ja3111797 | J. Am. Chem. Soc. 2012, 134, 20624–20627

(1.59 ppm), originating from the hydrogenation of cyclooctadiene. In addition, four transient peaks of low intensity were observed at 1.54, 5.62, 5.78, and 5.82 ppm in the 3−7 h reaction time range, which can be attributed to *cis*-cyclooctene and *cis,cis*-1,3-cyclooctadiene. Moreover, the alkyl groups of the silane precursor, namely $-(CH_2)_6-$ and $-CH_3$, presented significant changes in shape with reaction time, while their chemical shifts remained at 1.35 and 0.92 ppm, respectively. The asymmetric shape of the $-(CH_2)_6-$ signal is typically observed for micellar-type structure[17] and thus indicates significant octyl−octyl interactions. In the case of $Si-CH_2-$, the multiplet initially at 0.80 ppm is replaced by a broad peak at 0.73 ppm; this takes place with concomitant disappearance of the H_3Si- moiety. The line broadening of the peak at 0.73 ppm is consistent with a shorter transverse relaxation time (T_2), which is typically related to slower tumbling of a molecule and the attachment of this moiety to a larger object such as a nanoparticle/aggregate.[18] Note also that C_8 or linear hydrocarbon compounds such as octane or octene were not detected, indicating the absence of Si−C cleavage. These data indicate that the alkyl chain of the silane is part of the particles, which is probably responsible for their stability toward aggregation. Diffusion-ordered NMR spectroscopy (DOSY) performed on the colloid indicated a diffusion coefficient of the nickel−silicide nanoparticles $[Ni_xSi-C_8H_{17}]$ of 368 $\mu m^2/s$, while free silane showed a diffusion of 1776 $\mu m^2/s$ (Figure S3). Using the particle's diffusivity, a hydrodynamic diameter of ca. 2.6 nm was calculated, part of this diameter being related to the stabilizing octyl chain (which can be up to 1 nm long, *vide infra* for further comments).

In order to gain more insight into the structure of $[Ni_xSi-C_8H_{17}]$, X-ray absorption spectroscopy (XAS) was performed on pristine samples (handled under argon). The XANES spectra of bulk nickel(0) and nickel−silicide references are presented in Figure 2, together with the spectrum of the as-synthesized colloid dispersed on 184 m^2/g fumed silica (Evonik, ≥99.8%$_{Si}$), $[(Ni_xSi-C_8H_{17})/SiO_2]$, for ease of characterization. For all samples, the edge of X-ray adsorption is found starting at ca. 8331 eV, indicating a nickel oxidation state close to 0. This was confirmed by the absence of a white line at ca. 8350 eV, characteristic of oxides. Interestingly, the absorption spectrum of the supported $[Ni_xSi-C_8H_{17}]$ nanoparticles is significantly different from that of $Ni^{(0)}$, while the interferences observed are similar to those for Ni_2Si and, to a lower extent, $NiSi_2$. The absence of a Ni environment related to metallic nickel is in agreement with the possibility to record NMR spectra and the nonexistence of superparamagnetism from magnetism studies, excluding the formation of a Ni@silane core−shell structure.

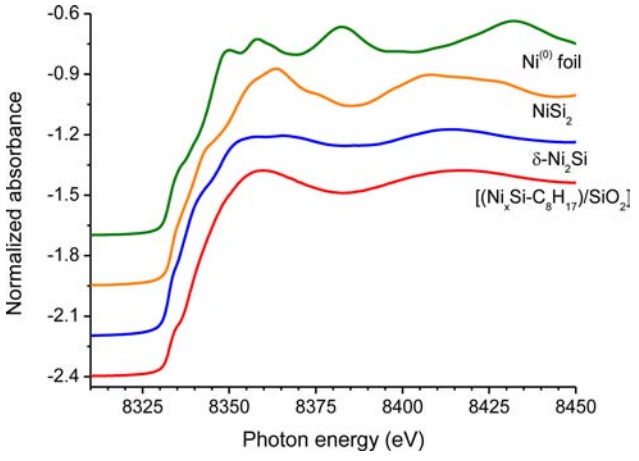

Figure 2. Normalized Ni K-edge near-edge XAS spectra of supported as-synthesized nickel−silane colloid, $NiSi_2$, Ni_2Si, and nickel foil.

The fit of the EXAFS spectrum, detailed in Table 1, gave average coordination numbers (N) for Ni in $[(Ni_xSi-C_8H_{17})/SiO_2]$ of 4.4 ± 0.9 silicon at 2.25 ± 0.02 Å and 2.8 ± 1 nickel at 2.45 ± 0.02 Å (Table 1). The number of nickel neighbors in the first shell of the as-synthesized nickel−silane nanoparticle does not fit with bulk nickel or δ-Ni_2Si, having respectively N = 12 and 8; no proper match between the neighbor distances is found either. However, both coordination numbers and neighbor distances fit remarkably with EXAFS data of reported amorphous nickel−silicide ($Si_{1-y}Ni_y$:H) prepared by sputtering, in particular Ni_3Si_2:H.[19] However, as the rupture of the Si−C bond from the octylsilane was not evidenced by liquid NMR, the formation of bulk nickel−silicide is unlikely. Instead, $Ni_xSi-C_8H_{17}$ probably corresponds to aggregates of small clusters stabilized by the alkyl group.

Table 1. EXAFS Fitting Parameters for $[(Ni_xSi-C_8H_{17})/SiO_2]$ and Several Related Ni-Based References

atom	coordination number[a] (N)	neighbor distance[a] (R, Å)	Debye−Waller factor[a] (σ^2, $\times10^{-3}$ Å^2)
$[(Ni_xSi-C_8H_{17})/SiO_2]$			
Si	4.4(9)	2.25(2)	15(3)
Ni	2.8(10)	2.45(1)	11(3)
δ-Ni_2Si			
Si	4	2.30(1)	7(1)
Ni	8	2.56(1)	8.6(6)
Si	1	2.60(5)	9.7(3)
Amorphous Ni_3Si_2[b]			
Si	5(2)	2.30(5)	8(3)
Ni	3(2)	2.45(3)	8(3)
$Ni^{(0)}$ foil			
Ni	12	2.48(1)	6(4)
Ni	6	3.49(2)	9.6(6)
Ni	24	4.32(1)	9.6*
Ni	12	4.97(1)	9.6*

[a]Numbers in parentheses correspond to the error on the last digit. [b]Extrapolated from ref 19.

Similarly to $[(Ni_xSi-C_8H_{17})/SiO_2]$, the reported amorphous nickel−silicides ($Si_{1-y}Ni_y$:H) do not present second or higher shells for Ni/Si ratio lower than 1.8 ($y \leq 0.71$). However, the composition dependence of the mean-square deviation in interatomic distances (σ^2) of the nickel−silane nanoparticles is significantly greater than for sputtered amorphous nickel−silicides. This is consistent with an important structure distortion in $[(Ni_xSi-C_8H_{17})/SiO_2]$ and/or the presence of smaller particles, in agreement with the formation of $Ni_xSi-C_8H_{17}$ aggregates.

dx.doi.org/10.1021/ja3111797 | J. Am. Chem. Soc. 2012, 134, 20624−20627

Interestingly, when the sample was heated under static hydrogen from 250 °C stepwise to 1000 °C, the silicon coordination number progressively decreased to 2.6 ± 1.1, while the nickel coordination number increased to 4.5 ± 1 (Table S4, Figure S5). Meanwhile, the average neighbor distance remained constant for Ni−Ni and increased slightly for Ni−Si. When compared to the XAS results of sputtered amorphous nickel−silicide ($Si_{1-y}Ni_y$:H),[19] the evolutions with heat treatment under H_2 reported here are consistent with the presence of an amorphous alloy richer in nickel than the initial particles (from a-Ni_3Si_2 to a-Ni_2Si), indicating a segregation of silicon from nickel. This phenomenon might originate from the reaction of silicon with the silica used to support the colloid and/or the hydrogenolysis of the alkyl chain and the consequent restructuring of the nanoparticle.

When $[Ni_xSi{-}C_8H_{17}]$ nanoparticles are exposed to oxygen or dry air, $[(Ni_xSi)O_y]$, the colloid turns from deep black to slightly yellow, which is likely related to the oxidation of Ni and Si (*vide infra*). Similarly to the as-synthesized colloid, no sedimentation was observed after several weeks. Transmission electron microscopy (TEM) indicated the presence of small isolated particles with a narrow particle size distribution centered at 2.4 ± 0.5 nm (Figure 3).

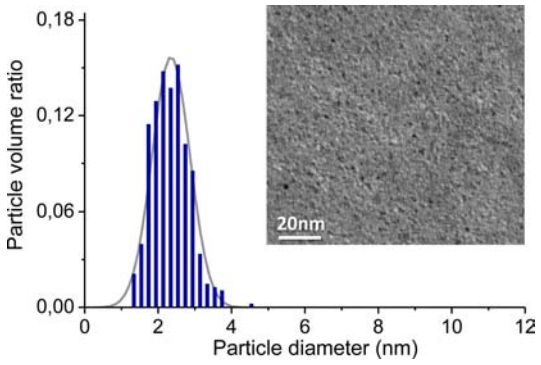

Figure 3. Representative TEM micrograph and corresponding particle size distribution of $[Ni_xSi{-}C_8H_{17}]$ after oxidization in air at room temperature.

The evolution of the nickel environment of $[(Ni_xSi{-}C_8H_{17})/SiO_2]$ with various treatments was monitored *ex situ* by XAS, and the spectra are presented in Figure 4. As a result of slow exposure of the as-synthesized particles to oxygen at room temperature, namely $[(Ni_xSi)O_y/SiO_2]$, a shift of the rising K-edge of nickel from 8331 to 8337 eV occurs, together with the appearance of a white line with a maximum at 8350 eV, consistent with the formation of nickel oxide (NiO).

Further treatment of $[(Ni_xSi)O_y/SiO_2]$ under hydrogen at 500 °C, $[Ni^0(Si_yO_z)/SiO_2]$, led to the disappearance of the white line (8350 eV) and a shift of the rising edge back to 8331 eV. However, the EXAFS interferences indicate that the nickel has an environment close to that of bulk $Ni^{(0)}$. In addition, the apparent coordination number of $[Ni^0(Si_yO_z)/SiO_2]$ is 7.6 ± 0.5, much lower than the values for 2.8 nm particles (N = 10.2 ± 0.5, not shown) and bulk nickel (N = 12), indicating an average Ni particle size significantly smaller than 2.8 nm.

Hydrogen chemisorption was performed on $[Ni^0(Si_yO_z)/SiO_2]$ having a Ni loading of 0.72 wt%, which showed a H_2 adsorption of 92 ± 3 mol_{H_2}/g_{cat}, indicating a nickel dispersion of 71 ± 5%. Assuming a H/Ni_{surf} ratio of 1[20] and the formation

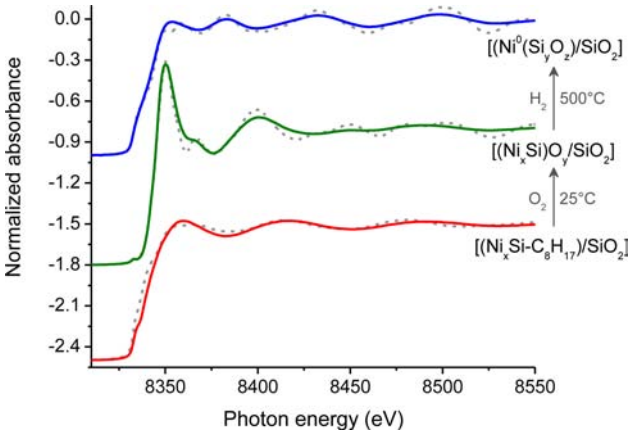

Figure 4. Normalized Ni K-edge near-edge EXAFS spectra of as-synthesized nickel−silane colloid supported on silica (red), exposed to O_2 at 20 °C (green) and further reduced under H_2 at 500 °C (blue). The gray dotted lines stand as references, respectively Ni_2Si, NiO, and $Ni^{(0)}$ foil.

of perfect truncated octahedral Ni particles,[21] this implies the presence of particles having an average size of 1.3 ± 0.2 nm.

This is consistent with the results of DOSY experiment (hydrodynamic diameter 2.6 nm, *vide supra*) and with the TEM observation of the oxidized $[Ni_xSi{-}C_8H_{17}]$ nanoparticles (2.4 nm, *vide supra*), taking into consideration the increase of molar volume upon oxidation (up to 90%). The mean particle size obtained by chemisorption was confirmed by a HAADF-STEM study, indicating an oxidized particle size in the 1−2.5 nm range (Figure 5). However, as a result of the low contrast of NiO_x compared to silica, no accurate particle size distribution could be obtained for $[Ni^0(Si_yO_z)/SiO_2]$.

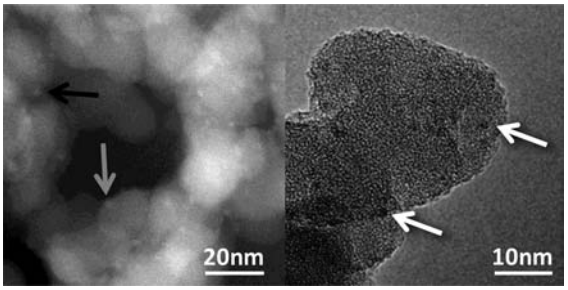

Figure 5. Pictures of $[Ni(Si_yO_z)/SiO_2]$, reduced at 500 °C under H_2 and slowly reoxidized. Left, HAADF−STEM; right, −200 kV HR-TEM.

The nickel−silica-based sample $[Ni^0(Si_yO_z)/SiO_2]$ was tested in DR of CH_4 at 500 °C and atmospheric pressure. This catalyst presented ca. 20% higher activity (465 $mol_{CO}/h{\cdot}mol_{tot.Ni}$ at steady state, Figure S6) when compared to a conventional Ni/SiO_2 catalyst (390 $mol_{CO}/h{\cdot}mol_{tot.Ni}$), its greater performance being directly proportional to the very high nickel dispersion of the nickel−silane-based nanoparticles, as expected for such a catalytic system.[22] However, these two catalysts suffered from a severe deactivation (80% loss) typical of Ni/SiO_2. Post-reaction TEM study indicated that particle sintering was responsible for a ca. 30% decrease of active sites while hardly any carbon deposition could be observed. This indicates that ca. 70% of the catalyst deactivation can be related to (sub)surface chemical deactivation (NiC_x, NiO_xH_y, ...).

dx.doi.org/10.1021/ja3111797 | J. Am. Chem. Soc. 2012, 134, 20624−20627

Since colloids can be easily dispersed on various oxides, we supported them on 58 m^2/g fumed ceria (Evonik, ≥99.5%Ce) [$Ni(Si_yO_z)/CeO_2$], which is known to improve the performance of reforming catalysts thanks to its high oxygen storage capacity.[23] This sample was subjected to the same procedure described for silica, i.e., subsequent oxidation and further H_2 treatment. This sample was compared with conventional Ni/CeO_2 catalyst [Ni_{NO_3}/CeO_2] prepared by incipient wetness impregnation (IWI).[24] Hydrogen chemisorption indicated similar nickel dispersion, i.e., 54 and 47% for [$Ni(Si_yO_z)/CeO_2$] and [Ni_{NO_3}/CeO_2], respectively, which is lower than when silica is used as a support. Comparing these systems in DR (Figure S6) indicates that both systems are more stable than the silica-supported homologue and that the nickel−silane approach gives a syngas productivity 60% higher than the traditional catalyst (710 vs 430 $mol_{CO}/h{\cdot}mol_{tot.Ni}$, Figure S6) and a 34% greater intrinsic activity (910 vs 680 $mol_{CO_2}/h{\cdot}mol_{surf.Ni}$,Table S7). A TEM study of the catalyst after the DR test hardly revealed any carbon, nickel sintering being unfortunately impossible to study. The greater stability of ceria-based catalysts can be related to a so-called stronger metal−support interaction,[25] which is likely to be influenced by the presence of silicon in [$Ni(Si_yO_z)/CeO_2$].

In conclusion, bis(cyclooctadiene)nickel(0) with octylsilane yields stable 2-nm narrowly distributed $Ni_x(Si{-}C_8H_{17})_y$ colloids. The nickel having originally an environment similar to that of amorphous nickel−silicide (Ni_3Si_2) is fully oxidized when exposed to oxygen at 20 °C. These colloids can be supported on silica or ceria and transformed into nickel(0) nanoparticles upon H_2 treatment with a remarkably high dispersion of 71 ± 5%, corresponding to 1.3 ± 0.2 nm Ni nanoparticles. These narrowly distributed supported particles are highly active and stable catalysts for dry reforming, in particular when supported on ceria. Overall, this approach opens a general route for nickel-based catalyst preparation on various supports, and we are currently exploring the generality of this approach.

■ ASSOCIATED CONTENT

Ⓢ Supporting Information

In situ liquid ^1H NMR study of colloid formation in THF at 55 °C; DOSY study of the as-synthesized colloid; fitting parameters for [$(Ni_xSi{-}C_8H_{17})/SiO_2$], [$(Ni_xSi)/SiO_2]^{H_2}{}_{500}$, [$(Ni_xSi)/SiO_2]^{H_2}{}_{1000}$, and several nickel−silicide references; average first-shell Ni coordination numbers obtained from Ni K-edge data for [$(Ni_xSi{-}C_8H_{17})/SiO_2$] as prepared and after heating under hydrogen at various temperatures; variation of [$Ni(Si_xO_z)/CeO_2$] and [Ni_{NO_3}/CeO_2] CO rate and TOF_{CO_2} in CO_2 reforming of CH_4 with time on stream; initial and steady-state TOF_{CO_2} of various Ni_x/SiO_2 catalysts during DR of methane at 773 K; and details of XAS study. This material is available free of charge via the Internet at http://pubs.acs.org.

■ AUTHOR INFORMATION

Corresponding Author

ccoperet@inorg.chem.ethz.ch; thieuleux@cpe.fr

Present Address

[†]Department of Chemistry, ETH Zürich

Notes

The authors declare no competing financial interest.

■ ACKNOWLEDGMENTS

ACENET and ETH Zürich are thanked for financial support.

■ REFERENCES

(1) Torres Galvis, H. M.; Bitter, J. H.; Davidian, T.; Ruitenbeek, M.; Dugulan, A. I.; de Jong, K. P. *J. Am. Chem. Soc.* **2012**, *134*, 16207.
(2) Shetty, S.; Jansen, A. P. J.; van Santen, R. A. *J. Am. Chem. Soc.* **2009**, *131*, 12874.
(3) den Breejen, J. P.; Radstake, P. B.; Bezemer, G. L.; Bitter, J. H.; Frøseth, V.; Holmen, A.; Jong, K. P. d. *J. Am. Chem. Soc.* **2009**, *131*, 7197.
(4) Rostrup-Nielsen, J. R. *Catal. Today* **1993**, *18*, 305.
(5) Ashcroft, A. T.; Cheetham, A. K.; Green, M. L. H.; Vernon, P. D. F. *Nature* **1991**, *352*, 225.
(6) Huber, G. W.; Shabaker, J. W.; Dumesic, J. A. *Science* **2003**, *300*, 2075.
(7) Besenbacher, F.; Chorkendorff, I.; Clausen, B. S.; Hammer, B.; Molenbroek, A. M.; Nørskov, J. K.; Stensgaard, I. *Science* **1998**, *279*, 1913.
(8) Zhou, G.; Barrio, L.; Agnoli, S.; Senanayake, S. D.; Evans, J.; Kubacka, A.; Estrella, M.; Hanson, J. C.; Martínez-Arias, A.; Fernández-García, M.; Rodriguez, J. A. *Angew. Chem., Int. Ed.* **2010**, *49*, 9680.
(9) Nikolla, E.; Holewinski, A.; Schwank, J.; Linic, S. J. *Am. Chem. Soc.* **2006**, *128*, 11354.
(10) Regalbuto, J. R. *Catalyst Preparation: Science and Engineering*; Taylor & Francis, 2007.
(11) Espinosa-Alonso, L.; O'Brien, M. G.; Jacques, S. D. M.; Beale, A. M.; de Jong, K. P.; Barnes, P.; Weckhuysen, B. M. *J. Am. Chem. Soc.* **2009**, *131*, 16932.
(12) Sietsma, J. R. A.; Meeldijk, J. D.; den Breejen, J. P.; Versluijs-Helder, M.; van Dillen, A. J.; de Jongh, P. E.; de Jong, K. P. *Angew. Chem., Int. Ed.* **2007**, *46*, 4547.
(13) van der Lee, M. K.; van Dillen, J.; Bitter, J. H.; de Jong, K. P. *J. Am. Chem. Soc.* **2005**, *127*, 13573.
(14) de Jong, K. P. *Synthesis of Solid Catalysts*; Wiley VCH: Weinheim, Germany, 2009.
(15) Pelzer, K.; Laleu, B.; Lefebvre, F.; Philippot, K.; Chaudret, B.; Candy, J. P.; Basset, J. M. *Chem. Mater.* **2004**, *16*, 4937.
(16) Boualleg, M.; Basset, J. M.; Candy, J. P.; Delichere, P.; Pelzer, K.; Veyre, L.; Thieuleux, C. *Chem. Mater.* **2009**, *21*, 775.
(17) Lemyre, J.-L.; Ritcey, A. M. *Langmuir* **2010**, *26*, 6250.
(18) Venters, R. A.; Thompson, R.; Cavanagh, J. *J. Mol. Struct.* **2002**, *602−603*, 275.
(19) Asal, R.; Baker, S. H.; Gurman, S. J.; Bayliss, S. C.; Davis, E. A. *J. Phys. Condens. Mat.* **1992**, *4*, 7169.
(20) Bartholomew, C. H.; Pannell, R. B. *J. Catal.* **1980**, *65*, 390.
(21) Borodziński, A.; Bonarowska, M. *Langmuir* **1997**, *13*, 5613.
(22) Baudouin, D.; Rodemerck, U.; Krumeich, F.; De Mallmann, A.; Szeto, K. C.; Ménard, H.; Veyre, L.; Candy, J. P.; Webb, P. B.; Thieuleux, C.; Copéret, C. *J. Catal.* **2013**, *297*, 27.
(23) Bradford, M. C. J.; Vannice, M. A. *Catal. Rev.* **1999**, *41*, 1.
(24) Sietsma, J. R. A.; Meeldijk, J. D.; Versluijs-Helder, M.; Broersma, A.; van Dillen, A. J.; de Jongh, P. E.; de Jong, K. P. *Chem. Mater.* **2008**, *20*, 2921.
(25) Gonzalez-DelaCruz, V. M.; Holgado, J. P.; Pereñíguez, R.; Caballero, A. *J. Catal.* **2008**, *257*, 307.